Present and Future of Modeling Global Environmental Change: Toward Integrated Modeling, Eds., T. Matsuno and H. Kida, pp. 15–28.
© by TERRAPUB, 2001.

Projections of Future Climate Change in the 21st Century Simulated by the CCSR/NIES CGCM under the IPCC SRES Scenarios

Toru NOZAWA[1], Seita EMORI[1], Atusi NUMAGUTI[2], Yoko TSUSHIMA[3], Toshihiko TAKEMURA[4], Teruyuki NAKAJIMA[4], Ayako ABE-OUCHI[4] and Masahide KIMOTO[4]

[1]*National Institute for Environmental Studies, Tsukuba, Ibaraki 305-8506, Japan*
[2]*Graduate School of Environmental Earth Science, Hokkaido University, Sapporo 060-0810, Japan*
[3]*Institute for Global Change Research, Frontier Research System for Global Change, Yokohama 236-0001, Japan*
[4]*Center for Climate System Research, University of Tokyo, Tokyo 153-8904, Japan*

Abstract—Transient coupled ocean-atmosphere model experiments based on the Special Report on Emission Scenarios (SRES) of the Intergovernmental Panel on Climate Change (IPCC) were done to investigate the direct and indirect climate impacts of the anthropogenic sulfate and carbonaceous aerosols in the future projections of climate change. The numerical simulations are carried out for all four illustrative "marker" scenarios of A1, A2, B1, and B2. Direct radiative forcing of the carbonaceous aerosols nearly cancels out that of the sulfate aerosols for all scenarios. Estimated total indirect radiative forcing is about –1.3 Wm^{-2} for the A1, B1, and B2 scenarios, and is about –2.0 Wm^{-2} for the A2 scenario in the latter half of the 21st century. Global and annual averages of the surface air temperature increase for all scenarios because of the dominance of the radiative forcing of the increased CO_2. The global warming is decelerated with an increase in the anthropogenic sulfate and carbonaceous aerosols, because the indirect forcing due to the aerosols has a significant cooling effect. The global mean temperature change in 2100 with respect to the 1961–90 average is the largest and is about 5.5°C for A2, whereas it is the smallest and is about 3.3°C for B1. Geographical distribution of the surface warming does not depend much on the scenarios. Cloud feedback becomes dominant in the latter half of the 21st century, which introduces further warming at the surface.

INTRODUCTION

The time-dependent climate response to the increasing greenhouse gases and anthropogenic sulfate aerosols has been investigated since the middle 1990s using the coupled ocean-atmosphere general circulation models (CGCMs). In most of the previous studies, the direct radiative forcing (DRF) of sulfate aerosols

was expressed as an equivalent change in surface albedo (Hasselmann *et al.*, 1995; Mitchell *et al.*, 1995; Haywood *et al.*, 1997; Mitchell and Johns, 1997). Because they assumed a globally uniform relative humidity of 80%, the DRF of sulfate was overestimated (underestimated) over the dry (wet) regions. On the other hand, Emori *et al.* (1999) carried out a CGCM experiment with an explicit representation of scattering and showed that the DRF of sulfate was overestimated in those studies using the equivalent albedo method.

In addition to the DRF, aerosols also introduce the indirect radiative forcing (IRF) which has a further cooling effect by increasing the brightness and the extent of clouds. The first attempt to include the IRF of sulfate aerosols into the transient CGCM experiments was done by Meehl *et al.* (1996). They modified the cloud albedo by multiplying a factor of 1.00 or 1.05 to represent the IRF of sulfate aerosols. Recently, Roeckner *et al.* (1999) calculated the sulfur cycle within their CGCM and studied the future climate change including the indirect effect of sulfate as well as the direct one. They showed that the surface warming is further reduced by including the cloud albedo effect and that the suppression of warming is observed not only in the Northern Hemisphere but also in the Southern Hemisphere.

In all previous studies, the concentrations of greenhouse gases and sulfate aerosols are increased according to the IS92a scenario (IPCC, 1992). However, the IS92a scenario is somewhat unrealistic at present; it was made on the basis of 1985 datasets and included neither the restructuring in Eastern Europe and the former Soviet Union nor the rapid economic growth of the Asian countries in 1990s. Moreover, the models do not include the radiative impacts of the tropospheric aerosols other than sulfate. Since IPCC (1996), it has been pointed out that the DRF of carbonaceous aerosols may be as large as that of sulfate, and there are a number of related studies (Haywood and Ramaswamy, 1998; Penner *et al.*, 1998; Grant *et al.*, 1999; Cooke *et al.*, 1999). According to Penner *et al.* (1998), for example, the estimated DRF of black carbon (BC) and organic carbon (OC) by fossil fuel combustion ranges from +0.16 to +0.20 Wm^{-2} while that by biomass burning ranges from –0.23 to –0.14 Wm^{-2}, although their uncertainty is very large. These two DRFs of carbonaceous aerosols are likely to cancel each other out on a global average. However, their geographical distributions are somewhat different; therefore, the radiative impact of carbonaceous aerosols should not be excluded.

In this study, we perform coupled ocean-atmosphere model experiments of future climate change including the climate impacts of various aerosols under a new set of the IPCC scenarios (IPCC, 2000). In addition to the radiative impact of sulfate aerosol, those of carbonaceous, sea salt, and soil dust aerosols are considered. The indirect radiative forcing due to cloud albedo and lifetime effects is considered by representing the cloud droplet number concentration as a function of the aerosol numbers. Future concentrations of greenhouse gases and anthropogenic aerosols follow the SRES scenarios.

NUMERICAL MODEL AND EXPERIMENTAL DESIGN

The model used here is an updated version of the Center for Climate System Research/National Institute for Environmental Studies (CCSR/NIES) CGCM used by Emori *et al*. (1999). From now on, we refer to the updated CGCM as CCSR/NIES2 and to the previous one as CCSR/NIES1. Although most of the dynamical and physical components of CCSR/NIES2 are exactly the same as those of CCSR/NIES1, some physical parameterizations are updated:

- Parameters for cumulus detrainment and ice cloud settling are adjusted to reduce excessive cloud radiative forcing (CRF) in the tropics.
- Gas absorption parameters in the radiation code are changed to represent better sensitivity to doubling CO_2 (Nakajima *et al*., 2000).
- Direct and indirect radiative effects of various aerosols are included, the details of which will be explained in the following.

The spatial resolution is about $5.6° \times 5.6°$ in the horizontal (the triangular truncation at wavenumber 21) and 20 levels in the vertical directions, respectively, for the atmospheric part, and about $2.8° \times 2.8°$ and 17 levels for the oceanic part. Flux adjustment for ocean-atmosphere heat and water exchange is applied to prevent a drift in the modeled climate.

Well-mixed greenhouse gases (WMGG) of CO_2, methane (CH_4), nitrous oxide (N_2O), and thirteen species of halocarbons are considered individually. We use three-dimensional (3-D) tropospheric ozone data, which are calculated by a 3-D Lagrangian chemistry transport model of the Hadley Centre for Climate Prediction and Research at the United Kingdom Meteorological Office (Collins *et al*., 1997).

The major four species of sulfate, carbonaceous, sea salt, and soil dust aerosols are considered. The mass and number concentrations of these aerosols are calculated offline by an aerosol transport model of CCSR (Takemura *et al*., 2000). Sulfate aerosol concentration is calculated from the anthropogenic, volcanic, and dimethylsulfide SO_2 emissions. The IPCC SRES gridded sulfur emission dataset is used for the anthropogenic SO_2 (IPCC, 2000), which is constructed from the Emission Database for Global Atmospheric Research, EDGAR V2.0 (Olivier *et al*., 1996). The sulfate aerosols are assumed to be 75% H_2SO_4 as in Emori *et al*. (1999). Carbonaceous aerosol concentration is calculated from the CO_2 emission by fossil fuel and biofuel combustions and that by biomass burning. The emission datasets for the carbonaceous aerosols are constructed mainly using the EDGAR V2.0 for the emission by fossil fuel and biofuel combustions, and the Global Emissions Inventory Activity, GEIA (Cooke and Wilson, 1996) for that by biomass burning. The carbonaceous aerosols are assumed to be an external mixture of three components which have different mixing ratios of BC/OC = 0.30, 0.15, and 0.00. Each component of these is further assumed to be an internal mixture of BC and OC. Optical properties of these four aerosols are determined by the same method as that adopted in Emori *et al*. (1999). The volumetric mode

Table 1. Volumetric mode radius in dry environment r_d and dispersion parameter of the log-normal distribution σ_g for each aerosol particle.

Species	r_d (μm)	σ_g
Sulfate	0.13	2.00
Carbonaceous	0.13	2.00
Sea salt	1.50	2.51
Soil dust	6.00	2.50

radius in the dry condition and the geometric standard deviation for a lognormal size distribution are listed in Table 1 for each aerosol. The hygroscopic growth of sulfate, carbonaceous, and sea salt aerosols is considered according to Shettle and Fenn (1979). The soil dust aerosols are assumed to be hydrophobic.

The cloud albedo and lifetime effects are considered through a simple relationship between the aerosol numbers and the cloud droplet number concentrations

$$N_c = \frac{\varepsilon N_a N_{\max}}{\varepsilon N_a + N_{\max}}, \tag{1}$$

where N_c is the cloud droplet number concentration, N_a the aerosol number concentration, ε a proportional coefficient, and $N_{\max}$ the upper limit of N_c. This relationship between N_c and N_a depends on two tuning parameters, ε and $N_{\max}$. Here, $\varepsilon = 1$ and $N_{\max} = 400$ cm^{-3} are adopted to fit Eq. (1) with the measurements by Martin *et al.* (1994). The total aerosol number N_a is given by the sum of the number concentrations of sulfate, carbonaceous, and sea salt aerosols, and its minimum, and the background value is set to 30 cm^{-3}. For liquid clouds, the effective radius of a cloud droplet is calculated from both the cloud water mixing ratio and the cloud droplet number concentration to include the cloud albedo effect (Jones *et al.*, 1994; Boucher and Lohmann, 1995). The cloud lifetime effect is also taken into consideration in the large-scale cloud parameterization as the autoconversion rate of cloud droplets following Berry (1967) as was introduced by Lohmann and Feichter (1997).

In a control experiment (CTL), the concentrations of WMGG are fixed at 1990 values, while the 1990 distributions of ozone and aerosols are given as climatology. After a fifty-year spinup, the CTL run is done for 280 years with constant flux adjustment. To make the initial state of the transient experiments equivalent to the pre-industrial time, the concentrations of WMGG, ozone, and aerosols are set to 1890 values and the distributions at year 30 of CTL, and another thirty-year run is done thereafter using the same flux adjustment as in CTL.

Time-dependent experiments are performed for the period between 1890 and 2100. The concentrations of greenhouse gases and anthropogenic aerosols are given following observational datasets before 1990 and thereafter following all

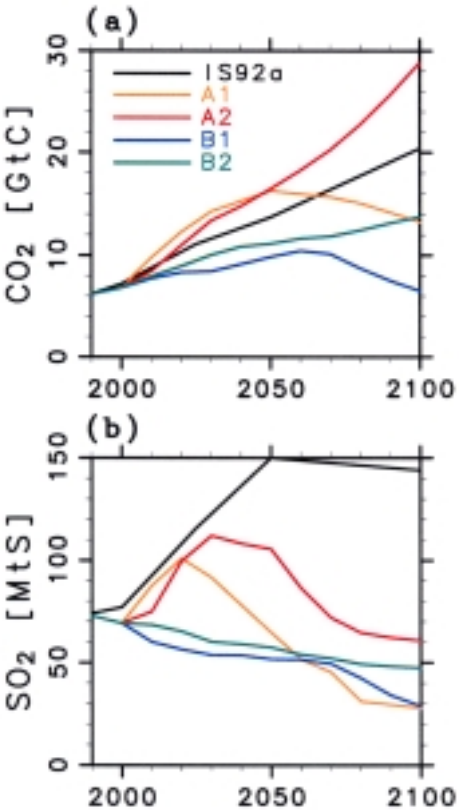

Fig. 1. Temporal variation in (a) CO_2 and (b) SO_2 emission by fossil fuel combustion for the IS92a and SRES "marker" scenarios.

four SRES "marker" scenarios (namely A1, A2, B1, and B2), which are representative of a wide spectrum of forty scenarios (IPCC, 2000). Figure 1 shows the temporal variations in (a) CO_2 and (b) SO_2 emission by fossil fuel combustion for the IS92a and SRES scenarios. Emission of CO_2 by fossil fuel combustion continues increasing in the 21st century for all scenarios, although it slightly decreases in the latter half of this period for A1 and B1 scenarios (Fig. 1(a)). Temporal evolutions of the fossil fuel SO_2 emission in SRES scenarios are considerably different from that in IS92a; even though the SO_2 emission increases during the next two or three decades for the A1 and A2 scenarios, it starts decreasing later in the 21st century, and in 2100, it falls short of the present-day value for all scenarios (Fig. 1(b)). Future concentrations of CO_2, CH_4, and N_2O follow the scenarios and continue increasing, except for the concentration of CH_4 which decreases in the latter half of the 21st century for the A1 scenario. On the other hand, temporal variations in halocarbons do not depend

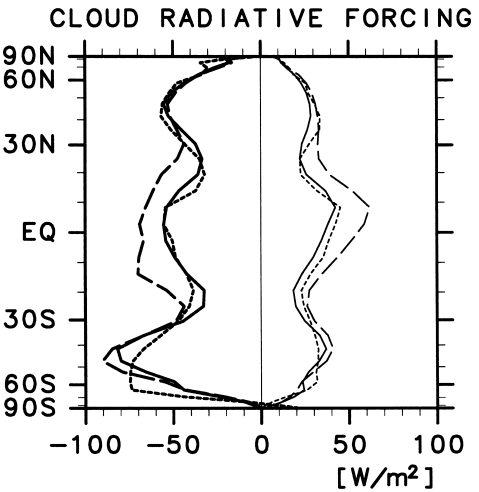

Fig. 2. Zonal mean shortwave (thick curves) and longwave (thin ones) cloud radiative forcing derived from control runs of CCSR/NIES2 (solid) and CCSR/NIES1 (long-dashed), and from satellite observation of ERBE (short-dashed).

on the scenarios. Changes in ozone concentrations are also considered to follow the scenarios by adding or subtracting the scaled pattern of projected ozone changes that are also provided by the Hadley Centre. Because the anthropogenic emissions of SO_2 and CO_2 follow the scenarios, future concentrations of sulfate and carbonaceous aerosols also vary depending on the scenarios. Concentrations of sea salt and soil dust aerosols are fixed at the present-day climatology because we have little information about their past and future changes.

RESULTS AND DISCUSSION

Figure 2 shows the zonal mean shortwave and longwave cloud radiative forcings (CRF) obtained in CTL (averages for the last 30 years). Magnitudes of the zonal mean CRFs in CCSR/NIES2 are reduced in almost all latitudes from those in CCSR/NIES1 by updating some physical parameterizations. In the middle and high latitudes of the Northern Hemisphere, the shortwave CRF in CCSR/NIES2 is slightly increased in comparison with that in CCSR/NIES1, which may be due to the inclusion of the indirect radiative effect of aerosols. As a result, the zonal mean CRFs in CCSR/NIES2 agree quite well with those derived from the satellite observation of Earth Radiation Budget Experiments, ERBE (Harrison *et al.*, 1990).

Radiative forcings due to an increase in greenhouse gases and anthropogenic aerosols from the pre-industrial to the present day are summarized in Table 2. These radiative forcings are identical to the instantaneous forcing (Hansen *et al.*, 1997) that is measured by net radiative flux change at the tropopause (assumed

Table 2. Global and annual mean instantaneous radiative forcing due to increases in greenhouse gases and anthropogenic aerosols from the pre-industrial era to the present day. Units are in Wm^{-2}. The tropopause level is assumed to be $\sigma = 0.1$ in the calculation. The cloud lifetime effect is computed as the difference in net fluxes at the tropopause between two independent simulations and therefore do not represent forcing in a strict sense.

	Radiative forcing (Wm^{-2})
Greenhouse gases	
CO_2	+1.57
CH_4	+0.36
N_2O	+0.21
Halocarbons	+0.26
Tropospheric ozone	+0.30
Aerosol (direct)	
Sulfate	–0.19
Carbonaceous	+0.07
Aerosol (indirect)	
Cloud albedo	–0.55
Cloud lifetime	–0.56

here to be $\sigma = 0.1$ level) in response to the perturbation under fixed meteorological fields. Another measure of radiative forcing is called adjusted forcing (Hansen *et al.*, 1997) which is adopted in IPCC (1996). On calculating the adjusted forcing, the stratospheric meteorological fields are allowed to adjust for the imposed perturbation with the tropospheric meteorological fields held fixed. Because the adjusted forcing is very difficult to compute and depends strongly on the choice of the tropopause level, we calculated the instantaneous forcing. Radiative forcing of CO_2 is calculated to be +1.57 Wm^{-2} and agrees quite well with its best guess, +1.56 Wm^{-2}, listed in table 2.2 of IPCC (1996), although the definition of these two forcings are slightly different. In the computation of the radiative forcing, we used the updated radiation parameters that are introduced to represent better sensitivity to doubling of CO_2. If we calculate the CO_2 forcing with the previous radiation parameters used in CCSR/NIES1, it is estimated to be +1.22 Wm^{-2}, indicating that the sensitivity to increased CO_2 is improved by updating the radiation parameters.

Although the direct radiative forcing of sulfate is somewhat small compared with the IPCC's best guess, it is nearly equal to the lower limit of the uncertainty range suggested in section 2.4.2.1 of IPCC (1996). Because we assumed that the loading of the biomass-burning aerosols does not vary in the past, the DRF of carbonaceous aerosols shown in Table 2 is only due to an increase in the fossil fuel BC and OC. The estimated carbonaceous forcing by the fossil-fuel combustion is within the range of uncertainty of the recent studies (Haywood and Ramaswamy, 1998; Penner *et al.*, 1998; Grant *et al.*, 1999; Cooke *et al.*, 1999). The cloud lifetime effect of aerosols is measured by the difference in cloud radiative

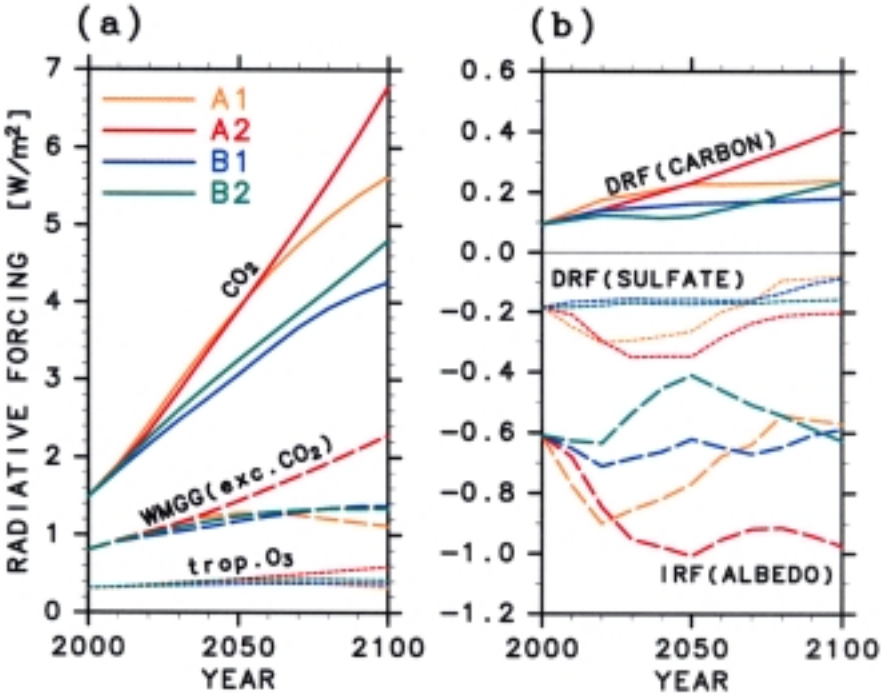

Fig. 3. Time series of global and annual mean radiative forcing of (a) greenhouse gases (thick solid, thick long-dashed, and thin short-dashed curves indicate the radiative forcing of CO_2, that of well-mixed greenhouse gases except CO_2, and that of tropospheric ozone, respectively) and (b) anthropogenic aerosols (thick solid, thin short-dashed, and thick long-dashed curves indicate the direct radiative forcing of carbonaceous aerosols, that of sulfate, and indirect radiative forcing due to the cloud albedo effect, respectively).

forcings at the tropopause between two independent simulations, one with the pre-industrial and the other with the present-day aerosols. Although the simulations are performed for 10 years to remove natural variability, the computed IRF due to the cloud lifetime effect may include some undesirable feedbacks and therefore does not represent a forcing in the strict sense. The indirect radiative forcing due to the cloud lifetime effect is estimated to be as large as that due to cloud albedo. This partitioning of the total indirect impact between the cloud albedo and the lifetime effect is close to that in Rotstayn (1999).

Figure 3 shows the time series of global and annual mean radiative forcings due to the changes in greenhouse gases and anthropogenic aerosols. The radiative forcing of greenhouse gases continues to increase in the future according to the scenarios. The radiative forcing of CO_2 is the largest and is about +6.8 Wm^{-2} for the A2 scenarios while it is the smallest and is about +4.3 Wm^{-2} for the B1 (solid curves in Fig. 3(a)). The global and annual mean DRF of sulfate is around –0.2

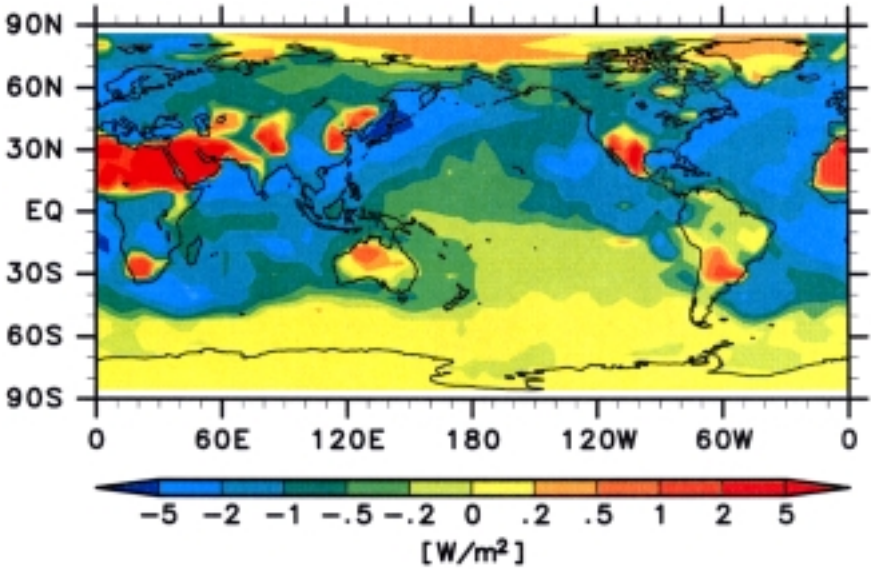

Fig. 4. Geographical distribution of annual mean total radiative forcing of aerosols (excluding the cloud lifetime effect) at 2100 for the A2 scenario.

Wm^{-2}, and its temporal variation follows the emission scenarios of SO_2 by fossil fuel combustion (thin short-dashed curves in Fig. 3(b)). The direct radiative forcing of carbonaceous aerosols slightly increases from +0.09 Wm^{-2} in 2000 to about +0.3 Wm^{-2} in 2100 following the emission scenarios of CO_2 (thick solid curves in Fig. 3(b)). Roughly speaking, the DRF of sulfate and carbonaceous aerosols nearly cancel each other, although there are some differences among the scenarios. The indirect radiative forcing due to the cloud albedo effect is around –0.65 Wm^{-2} for A1, B1, and B2, whereas it is around –1.0 Wm^{-2} for A2. The sulfate aerosols decrease while the carbonaceous aerosols increase in the 21st century; hence, the species most contributing to the IRF due to the cloud albedo effect is changed from the sulfate to the carbonaceous aerosol. As a result, the IRF remains nearly constant in the future. Assuming that the cloud lifetime effect is as large as that due to cloud albedo based on Table 2, total indirect radiative forcing is about –1.3 Wm^{-2} for A1, B1, and B2 and is about –2.0 Wm^{-2} for A2 in the latter half of the 21st century.

The geographical distribution of total radiative forcing of aerosols except for the cloud lifetime effect in the year 2100 is shown in Fig. 4 for the A2 scenario. The radiative forcing is negative in most of the world because the cloud albedo effect is dominant (Fig. 3(b)). There are some positive patches over land where the DRF of carbonaceous aerosols is dominant. Although the amplitude of the radiative forcing of aerosols is somewhat different among the scenarios, the geographical distribution does not depend very much on the scenarios.

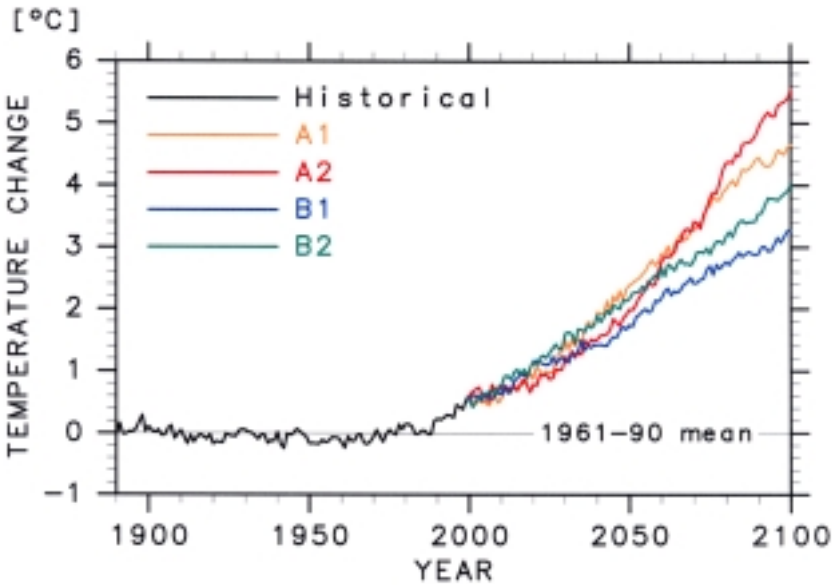

Fig. 5. Temporal evolutions of global and annual mean surface air temperature change with respect to the 1961–90 average (13.7°C).

Figure 5 shows future projections of the global and annual mean surface air temperature changes. The projected surface air temperature increases for all scenarios because the radiative forcing of increased CO_2 is dominant. The surface warming in the early 21st century is not greatly different among the scenarios. At this period, the CO_2 forcing is not so strong, although the IRF of aerosols has a significant cooling effect (thick long-dashed curves in Fig. 3(b)). Therefore, the global warming is decelerated with an increase in the anthropogenic sulfate and carbonaceous aerosols. The global mean temperature change in 2100 with respect to the 1961–90 average is the largest and is about 5.5°C for the A2 scenario, whereas it is the smallest and is about 3.3°C for the B1. The geographic pattern of the surface warming does not vary much among the scenarios; the warming is large over the land in the Northern Hemisphere and small around the Circumpolar Ocean of Southern Hemisphere (not shown). This is because the radiative impact of aerosols, which may cause geographical differences, is weaker than that of CO_2.

Figures 6(a) and (b) show the time series of the global and annual mean longwave and shortwave CRF. The longwave CRF remains nearly constant for all scenarios (Fig. 6(a)). On the other hand, the shortwave CRF increases after 2050 and, for the A1 and A2 scenarios, it increases rapidly from 2060 to 2080 (Fig. 6(b)). Figure 6(c) shows the temporal evolution of changes in zonal mean shortwave CRF with respect to the 1961–90 averages for the A2 scenario. By the year 2060, the shortwave CRF increases in the middle latitudes but decreases in

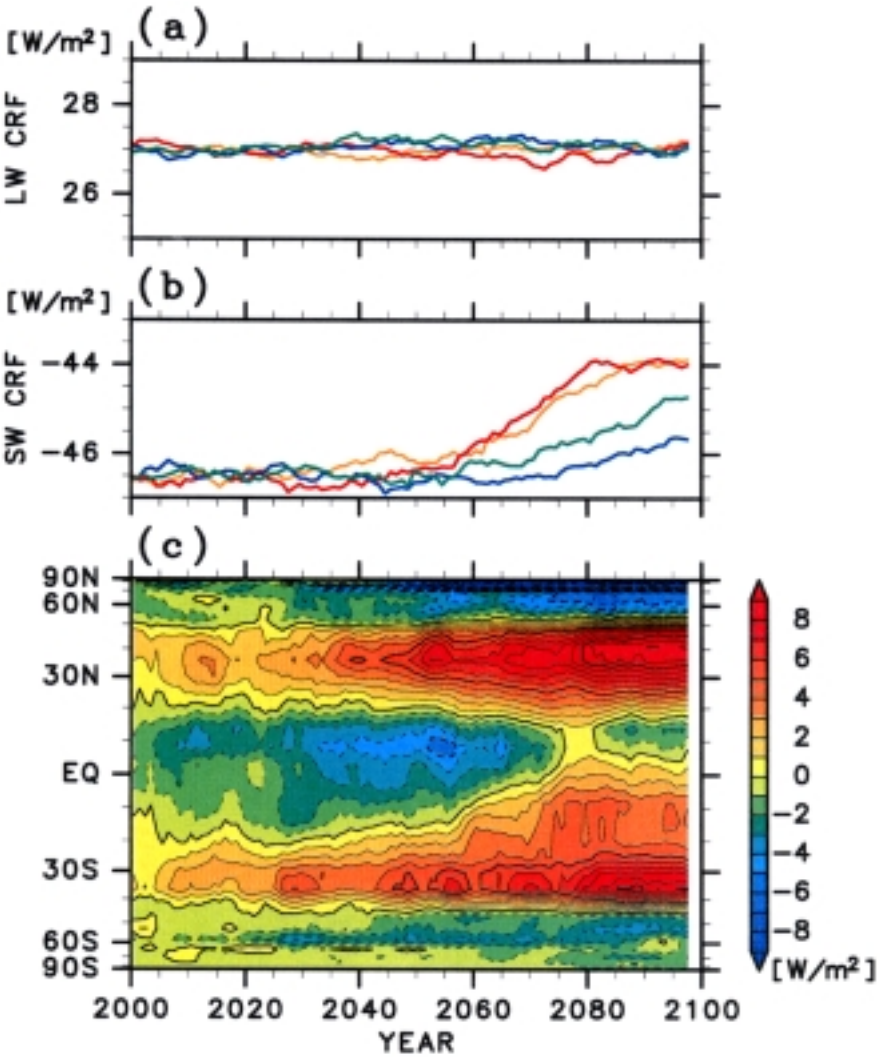

Fig. 6. Time series of global and annual mean (a) longwave and (b) shortwave cloud radiative forcing for all scenarios (the same color is adopted to indicate each scenario as in Figs. 1, 3 and 5), and (c) temporal evolution of the changes in shortwave cloud radiative forcing with respect to the 1961–90 mean for the A2 scenario. Five-year moving average is applied.

the tropics; therefore, it does not vary much for this period on a global average. On the other hand, the shortwave CRF increases in the middle and low latitudes, thereafter resulting in an increase in the global average (Fig. 6(b)). This rapid increase in the shortwave CRF accelerates the surface air temperature trend in the latter half of the 21st century. The detail of this cloud feedback is being analyzed

and will be reported elsewhere.

As seen in Fig. 5, the amount of global warming reported here may be greater than expected. For the case of a 1% per year increase in CO_2, the global mean surface air temperature change at the time of CO_2 doubling is about 3.2°C in CCSR/NIES2, whereas it is about 2.0°C in CCSR/NIES1. After diagnosing the models, we found that the large sensitivity of CCSR/NIES2 in comparison with CCSR/NIES1 is due to two factors: (i) use of another set of absorption parameters for various gases in the radiation code, and (ii) a difference in cloud feedback (positive in CCSR/NIES2 but negative in CCSR/NIES1) due to fine tuning of the parameters. According to a set of AGCM-mixed-layer ocean experiments, two-thirds of the increased sensitivity is explained by (i) and the rest by (ii) above, roughly speaking. For example, the global mean temperature change in 2100 with respect to the 1961–90 average is about 4.5°C and 2.6°C for A2 and B1 scenarios, respectively, in another set of SRES scenario runs (performed with CCSR/NIES2 except for the use of radiation parameters of CCSR/NIES1). Details on the climate sensitivity of the CCSR/NIES CGCMs will be reported in another paper (Abe-Ouchi *et al.*, 2001).

CONCLUSIONS

Transient climate change experiments were carried out using a coupled ocean-atmosphere model to investigate the future climate response to increasing greenhouse gases and to varying anthropogenic aerosols. Future concentrations of greenhouse gases are given according to the IPCC SRES "marker" scenarios. Direct and indirect radiative effects were considered for major four species of sulfate, carbonaceous, sea salt, and soil dust aerosols. Spatial distributions of sulfate and carbonaceous aerosols were calculated by an aerosol transport model of the Center for Climate System Research, University of Tokyo (Takemura *et al.*, 2000) from the datasets of anthropogenic SO_2 and CO_2 emissions that follow the scenarios.

The direct radiative forcings of sulfate and carbonaceous aerosols largely cancel each other. Two indirect forcings of anthropogenic aerosols, one due to the cloud albedo and the other due to the cloud lifetime effect, were estimated to be almost equal in magnitude at the present day. Assuming that the cloud lifetime effect is as large as that of cloud albedo in the future, total indirect forcing is about -1.3 Wm^{-2} for the A1, B1, and B2 scenarios, and is about -2.0 Wm^{-2} for the A2 scenario in the latter half of the 21st century. Global and annual averages of the surface air temperature increase for all scenarios. The global warming is decelerated with an increase in the anthropogenic sulfate and carbonaceous aerosols, because the indirect forcing due to these aerosols has a significant cooling effect in the early 21st century. The global and annual mean surface air temperature change in 2100 with respect to the 1961–90 average is the largest and is about 5.5°C for the A2 scenario, whereas it is the smallest and is about 3.3°C for the B1. Geographical distribution of the surface warming does not greatly depend on the scenarios. Cloud feedback accelerates the warming in the latter half of the 21st century.

Acknowledgments—We wish to thank Y. Yamanaka, N. Suginohara, and H. Okamoto for the model development and H. Kanzawa and A. Sumi for valuable discussions and encouragement. Thanks are also due to T. Johns for providing the tropospheric ozone data, to T. Masui and T. Morita for advising the handling of the CO_2 emission scenarios, and to S. Smith for advising the gridding procedure of the emission data. This work was partially supported by the Global Environment Research Program of the Environmental Agency of Japan. The calculations were done on an NEC SX-4 computer in the Center for Global Environment Research. The GFD-DENNOU Library was used for the drawings.

REFERENCE

Abe-Ouchi, A., M. Kimoto, T. Nakajima, T. Takemura, T. Nozawa, S. Emori, A. Numaguti and Y. Tsushima, 2001: On the climate sensitivity of the CCSR/NIES coupled ocean-atmosphere model, *J. Meteor. Soc. Japan* (to be submitted).

Berry, E. X., 1967: Cloud droplet growth by collection, *J. Atmos. Sci.*, **24**, 688–701.

Boucher, O. and U. Lohmann, 1995: The sulfate-CCN-cloud albedo effect: A sensitivity study with two general circulation models, *Tellus*, **47B**, 281–300.

Collins, W. J., D. S. Stevenson, C. E. Johnson and R. G. Derwent, 1997: Tropospheric ozone in a global-scale three-dimensional Lagrangian model and its response to NO_x emission controls, *J. Atmos. Chem.*, **26**, 223–274.

Cooke, W. F. and J. J. N. Wilson, 1996: A global black carbon aerosol model, *J. Geophys. Res.*, **101**, 19,395–19,409.

Cooke, W. F., C. Liousse, H. Cachier and J. Feichter, 1999: Construction of a $1° \times 1°$ fossil fuel emission data set for carbonaceous aerosol and implementation and radiative impact in the ECHAM4 model, *J. Geophys. Res.*, **104**, 22,137–22,162.

Emori, S., T. Nozawa, A. Abe-Ouchi, A. Numaguti, M. Kimoto and T. Nakajima, 1999: Coupled ocean-atmosphere model experiments of future climate change with an explicit representation of sulfate aerosol scattering, *J. Meteor. Soc. Japan*, **77**, 1299–1307.

Grant, K. E., C. C. Chuang, A. S. Grossman and J. E. Penner, 1999: Modeling the spectral optical properties of ammonium sulfate and biomass burning aerosols: Parameterization of relative humidity effects and model results, *Atmos. Environ.*, **33**, 2603–2620.

Hansen, J., M. Sato and R. Ruedy, 1997: Radiative forcing and climate response, *J. Geophys. Res.*, **102**, 6831–6864.

Harrison, E. F., P. Minnis, B. R. Barkstorm, V. Ramanathan, R. C. Cess and G. G. Gibson, 1990: Seasonal variation of cloud radiative forcing derived from the Earth Radiation Budget Experiment, *J. Geophys. Res.*, **95**, 18,687–18,703.

Hasselmann, K., L. Bengtsson, U. Cubasch, G. C. Hegerl, H. Rodhe, E. Roeckner, H. von Stroch, R. Voss and J. Waszkewitz, 1995: Detection of anthropogenic climate change using a fingerprint method, Technical report, Max-Planck-Institute fur Meteorologie Report No. 168, Hamburg, 24 pp.

Haywood, J. M. and V. Ramaswamy, 1998: Global sensitivity studies of the direct radiative forcing due to anthropogenic sulfate and black carbon aerosols, *J. Geophys. Res.*, **103**, 1562–1577.

Haywood, J. M., R. J. Stouffer, R. T. Wetherald, S. Manabe and V. Ramaswamy, 1997: Transient response of a coupled model to estimated changes in greenhouse gas and sulfate concentrations, *Geophys. Res. Lett.*, **24**, 1335–1338.

IPCC (Intergovernmental Panel on Climate Change), 1992: *Climate Change 1992: The Supplementary Report to the IPCC Scientific Assessment*, Houghton, J. H., B. A. Callander and S. K. Varney (eds.), Cambridge University Press, Cambridge, U.K., 205 pp.

IPCC, 1996: *Climate Change 1995: The Science of Climate Change*, Houghton J. H., L. G. Meira Filho, B. A. Callander, N. Harris, A. Kattenberg and K. Maskell (eds.), Cambridge University Press, Cambridge, U.K., 572 pp.

IPCC, 2000: *Special Report on Emissions Scenarios*, Nakicenovic N. and R. Swart (eds.), Cambridge University Press, Cambridge, U.K., 612 pp.

Jones, A., D. L. Roberts and A. Slingo, 1994: A climate model study of indirect radiative forcing by anthropogenic sulfate aerosols, *Nature*, **370**, 450–453.

Lohmann, U. and J. Feichter, 1997: Impact of sulfate aerosols on albedo and lifetime of clouds: A sensitivity study with the ECHAM4 GCM, *J. Geophys. Res.*, **102**, 13,685–13,700.

Martin, G. M., D. W. Johnson and A. Spice, 1994: The measurement and parameterization of effective radius of droplets in warm stratocumulus clouds, *J. Atmos. Sci.*, **51**, 1823–1842.

Meehl, G. A., W. M. Washington, D. J. Erickson, III, B. P. Briegleb and P. J. Jaumann, 1996: Climate change from increased CO_2 and direct and indirect effects of sulfate aerosols, *Geophys. Res. Lett.*, **23**, 3755–3758.

Mitchell, J. F. B. and T. C. Johns, 1997: On modification of global warming by sulphate aerosols, *J. Clim.*, **10**, 245–267.

Mitchell, J. F. B., T. C. Johns, J. M. Gregory and S. F. B. Tett, 1995: Climate response to increasing levels of greenhouse gases and sulfate aerosols, *Nature*, **376**, 501–504.

Nakajima, T., M. Tsukamoto, Y. Tsushima, A. Numaguti and T. Kimura, 2000: Modeling of the radiative process in an atmospheric general circulation model, *Apple. Opt.*, **39**, 4869–4878.

Olivier, J. G. J., A. F. Bouwman, C. W. M. van der Maas, J. J. M. Berdowski, C. Veldt, J. P. J. Bloos, A. J. H. Visschedijk, P. Y. J. Zandveld and J. L. Haverlag, 1996: Description of EDGAR version 2.0. a set of global emission inventories of greenhouse gases and ozone-depleting substances for anthropogenic and most natural sources on a per country basis and $1° \times 1°$ grid, Technical report, RIVM report nr. 771060 002 (TNO-MEP report nr. R96/119), 171 pp.

Penner, J. E., C. C. Chuang and K. Grant, 1998: Climate forcing by carbonaceous and sulfate aerosols, *Clim. Dyn.*, **14**, 839–851.

Roeckner, E., L. Bengtsson, J. Feichter, J. Lelieveld and H. Rodhe, 1999: Transient climate change simulations with a coupled atmosphere-ocean GCM including the tropospheric sulfur cycle, *J. Clim.*, **12**, 3004–3032.

Rotstayn, L. D., 1999: Indirect forcing by anthropogenic aerosols: A global climate model calculation of the effective-radius and cloud-lifetime effects, *J. Geophys. Res.*, **104**, 9369–9380.

Shettle, E. P. and R. W. Fenn, 1979: Models for the aerosols of the lower atmosphere and the effects of humidity variations on their optical properties, Technical report, Environmental Research Papers, No. 676, Air Force Geophysics Laboratory, U.S.A., 94 pp.

Takemura, T., H. Okamoto, Y. Maruyama, A. Numaguti, A. Higurashi and T. Nakajima, 2000: Global simulation of aerosol optical thickness distribution of various origins with a three-dimensional model, *J. Geophys. Res.*, **105**, 17,853–17,873.

T. Nozawa (e-mail: nozawa@nies.go.jp), S. Emori, A. Numaguti, Y. Tsushima, T. Takemura, T. Nakajima, A. Abe-Ouchi and M. Kimoto